NASA TECHNICAL MEMORANDUM

NASA TM X-2535

NASA TM X-2535

SUBSONIC PRESSURE DISTRIBUTIONS AROUND A SOLID MODEL OF AN INFLATABLE DECELERATOR ATTACHED TO THE BASE OF AN OGIVE-CYLINDER

by James Wayne Sawyer

Langley Research Center
Hampton, Va. 23365

NATIONAL AERONAUTICS AND SPACE ADMINISTRATION • WASHINGTON, D. C. • APRIL 1972

1. Report No.	2. Government Accession No.	3. Recipient's Catalog No.
NASA TM X-2535		

4. Title and Subtitle	5. Report Date
SUBSONIC PRESSURE DISTRIBUTIONS AROUND A SOLID MODEL OF AN INFLATABLE DECELERATOR ATTACHED TO THE BASE OF AN OGIVE-CYLINDER	April 1972
	6. Performing Organization Code

7. Author(s)	8. Performing Organization Report No.
James Wayne Sawyer	L-8188
	10. Work Unit No.
9. Performing Organization Name and Address	114-08-10-01
NASA Langley Research Center Hampton, Va. 23365	11. Contract or Grant No.
	13. Type of Report and Period Covered
12. Sponsoring Agency Name and Address	Technical Memorandum
National Aeronautics and Space Administration Washington, D.C. 20546	14. Sponsoring Agency Code

15. Supplementary Notes

16. Abstract

A wind-tunnel investigation was conducted at free-stream Mach numbers from 0.20 to 1.00 and corresponding Reynolds numbers, based on maximum afterbody diameter, from 2.25×10^6 to 6.90×10^6 on a solid model of an attached inflatable decelerator (AID) connected to the base of an ogive-cylinder. Tests were conducted to obtain ram-air and surface pressure distributions about the AID. AID shapes derived for subsonic deployment are dependent on the pressure distributions used in their derivation, and the different shapes obtained are dependent on the Mach number for which the design is made. The resulting pressure distributions were used in a design program to obtain new shapes which were compared with the original pressure-distribution shape.

17. Key Words (Suggested by Author(s))	18. Distribution Statement
Attached inflatable decelerators Pressure distributions Subsonic flow Ogive-cylinder	Unclassified – Unlimited

19. Security Classif. (of this report)	20. Security Classif. (of this page)	21. No. of Pages	22. Price*
Unclassified	Unclassified	29	$3.00

*For sale by the National Technical Information Service, Springfield, Virginia 22151

SUBSONIC PRESSURE DISTRIBUTIONS AROUND A SOLID MODEL OF AN INFLATABLE DECELERATOR ATTACHED TO THE BASE OF AN OGIVE-CYLINDER

By James Wayne Sawyer
Langley Research Center

SUMMARY

A wind-tunnel investigation was conducted at Mach numbers from 0.20 to 1.00 on a solid model of an attached inflatable decelerator (AID) connected to the base of an ogive-cylinder. Tests were conducted to obtain ram-air and surface pressure distributions about the AID. AID shapes derived for subsonic deployment are dependent on the pressure distributions used in their derivation, and the different shapes obtained are dependent on the Mach number for which the design is made. The experimental pressure distributions were used in a design program to obtain new shapes which were compared with the original pressure-distribution shape.

The results indicated that a separated flow region exists in the area of the cylinder-AID intersection. However, downstream of the point where the flow reattaches to the AID, the surface pressure distributions are similar to those obtained without the ogive-cylinder forebody present. Ram-air pressures obtained over most of the front surface of the AID are less than free-stream total pressure.

INTRODUCTION

The attached inflatable decelerator (AID) concept discussed in references 1 to 10 has been considered for use on several entry systems. One such system described in reference 11 has the AID attached to the base of an ogive-cylinder store which may be launched from an aircraft flying at subsonic or low transonic speeds. After release of the store from the carrier aircraft, the flexible AID (generally coated cloth) is deployed to reduce the store speed and change the flight trajectory.

Considerable design and development work has been done on the AID (see, for example, refs. 1 to 10), but most of the work was done with the AID attached to a large angle conical forebody and with the primary emphasis on deployment at supersonic speeds. During the investigation of reference 11, it became evident that additional surface-pressure data were needed to design an AID for deployment at low transonic speeds.

Thus for subsequent use in the study of reference 11, the present investigation was conducted to obtain preliminary ram-air and surface pressure distributions on a representative AID shape at subsonic and transonic speeds. A solid sting-mounted pressure model of an AID attached to the base of an ogive-cylinder was tested in the Langley 16-foot transonic tunnel. The resulting pressure distributions were used in the design program (described in ref. 2) to obtain first generation AID shapes designed for deployment at subsonic and transonic speeds. A comparison is made between the resulting design shapes and the original shape for which the pressure distributions were obtained.

Tests were conducted at free-stream Mach numbers between 0.20 and 1.00 and corresponding Reynolds numbers, based on the afterbody maximum diameter, from 2.25×10^6 to 6.90×10^6.

SYMBOLS

C_D pressure drag coefficient, $2\int_{r_i}^{1} C_{p,f}\left(\frac{r}{r_b'}\right)d\left(\frac{r}{r_b'}\right) - 2\int_{r_i}^{1} C_{p,b}\left(\frac{r}{r_b'}\right)d\left(\frac{r}{r_b'}\right)$

C_p surface pressure coefficient, $\frac{p_l - p_\infty}{q_\infty}$

$C_{p,f}$ pressure coefficient, front surface

$C_{p,b}$ pressure coefficient, base

l ogive-cylinder length

M_∞ free-stream Mach number

p_l local surface pressure

p_r ram-air pressure

p_t free-stream total pressure

p_∞ free-stream static pressure

q_∞ free-stream dynamic pressure

R Reynolds number based on $2r_b$

r	radial coordinate (fig. 1)
r_b	maximum radius of AID exclusive of burble fence (fig. 1), 25.40 cm
r_b'	maximum radius of burble fence (fig. 1), $1.10r_b$
r_c	radius of ogive-cylinder
r_i	dimensionless inside radius, $\frac{r_c}{r_b'}$ or $\frac{r_b}{r_b'}$
x	axial coordinate (fig. 1)
x'	axial coordinate measured from maximum radius of AID (fig. 7)

MODELS, FACILITIES, AND TESTS

Model

A sketch of the pressure-distribution model is shown in figure 1. The forebody was an ogive-cylinder with a cylinder radius of $0.11r_b$ (r_b is maximum radius of AID exclusive of burble fence) and a length of $2.79r_b$. The forebody was constructed of aluminum and machined to a finish smooth to the touch. The AID model and the burble fence had the same shapes as the ones used in the investigations of references 6 and 10 and were designed for deployment at a Mach number of 3.0. The solid model was constructed of cherry wood, impregnated with epoxy resin, and polished. The maximum radius of the burble fence was $1.10r_b$, and its leading edge was $0.045r_b$ upstream of the maximum radius of the AID. A sting with a radius of $0.10r_b$ was used to hold the model in the tunnel. The AID and burble fence coordinates are given in table I.

Static and ram-air pressure orifices were installed in the model at the locations indicated in figure 1; the locations of the static and ram-air pressure orifices are listed in tables I and II, respectively. Static pressures were measured at three stations on the forebody near its juncture with the afterbody, at 43 stations around the AID, and at 11 stations around the burble fence. These orifices were located in a plane containing the model axis. Ram-air pressures were measured at five stations along the AID at a distance of $0.03r_b$ above the surface. These orifices were staggered circumferentially to avoid mutual interference.

Facilities

The present investigation was conducted in the Langley 16-foot transonic tunnel, which is a single-return continuous-flow wind tunnel operating at atmospheric stagnation pressure. The slotted octagonal test section is 4.73 meters across the flats and may be operated continuously at Mach numbers from approximately 0.2 to 1.3. Reference 12 contains a description of the tunnel and its main drive system for Mach numbers below 1.10.

The data acquistion system utilized in this investigation consisted of three automatic pressure scanner units with 48 pressure channels in each unit. Each pressure scanner was connected to a strain-gage pressure transducer calibrated within ±350 newtons per square meter. All model pressures were recorded by operating each scanner unit at a scan rate of two channels per second. The output from the transducers was recorded and reduced to coefficient form at the Langley central digital data recording facility.

Tests

Tests were conducted with the model oriented at 0^{o} incidence with respect to the flow direction, and the Mach number was varied between 0.20 and 1.00. The test procedure consisted of slowly increasing the tunnel velocity until the desired test Mach number was reached. After the flow conditions had stabilized, the necessary data were taken and the Mach number was then increased to the next higher test condition. This procedure was repeated until the maximum Mach number was obtained; then a similar procedure was followed at a few check points as the Mach number was decreased. Data were taken at increasing Mach numbers of 0.20, 0.30, 0.40, 0.50, 0.60, 0.70, 0.80, 0.85, 0.90, 0.95, and 1.00, and the check points were made at decreasing Mach numbers of 0.80, 0.60, 0.40, and 0.20. The resulting Reynolds numbers, based on the maximum afterbody diameter $(2r_b)$, varied between 2.25×10^6 and 6.90×10^6, as indicated by the curve shown in figure 2. The Reynolds number for a given Mach number differed, depending on the direction from which the test condition was approached. The variation in Reynolds number results from a change in the temperature of the airstream with time during tunnel operation.

RESULTS AND DISCUSSION

Pressure-Distribution Tests

All surface pressure coefficients and ram-air pressure ratios obtained on the AID and the burble fence are given in tables I and II. A typical surface-pressure-coefficient distribution for a free-stream Mach number of 0.70 is shown in figure 3, where the values of C_p are represented by scaled arrows perpendicular to the configuration surface. Arrows pointing toward and away from the configuration surface indicate positive and

negative values of C_p, respectively. A relatively constant pressure-coefficient distribution is obtained on a portion of the front of the AID and over the base. For increasing AID radius outside the constant pressure region, the values of C_p first increase to a maximum value and then start to decrease. Downstream of the maximum C_p, the pressure-coefficient distribution follows a trend almost the same as that presented in reference 10 for the same configuration and flow conditions but without the ogive-cylinder attached. The constant pressure region on the front portion of the AID and on its base are indicative of separated flow. The separated flow region on the front portion of the AID is caused by an increase in pressure resulting from the abrupt change in surface contour at the juncture of the cylinder and the AID.

The effect of varying the free-stream Mach number may be seen in figure 4 where C_p is shown as a function of r/r_b for each Mach number investigated. Data taken after approaching the Mach number from either a smaller or larger value are presented for those Mach numbers for which both sets of data were taken. The separated flow region at the juncture of the cylinder and the AID as determined by the distributions of C_p is assumed to cover the region from the edge of the cylinder out to the maximum value of C_p $\left(0.15 \leqq r/r_b \leqq 0.5\right)$ where it is further assumed the flow reattaches to the body. Variations in the free-stream Mach number resulted in only slight changes in the extent of the separated flow region which first decreased and then increased slightly with increasing Mach number. Increasing the free-stream Mach number also resulted in higher values of C_p in the separated flow region and at the point where the flow attaches to the AID. Downstream of the assumed flow attachment point the variations of C_p with r/r_b and M_∞ are similar to those presented in reference 10 for the basic AID. Figures 4(a), 4(c), 4(e), and 4(g) indicate that the data obtained when approaching the Mach number from a smaller value are in good agreement with the data obtained when approaching the Mach number from a larger value; the only exception being at small Mach numbers where slight differences are obtained in the C_p values near the separated flow region at the cylinder-AID juncture.

Ram-air pressure ratios are shown in figure 5 as a function of r/r_b for selected Mach numbers throughout the range tested. The results indicate that ram-air pressures obtained over most of the forward surface of the AID are less than free-stream total pressure. Lower values of p_r/p_t are obtained for increasing Mach number and for decreasing values of r/r_b on the front of the AID. For the ram orifice located at approximately the edge of the separated region at the cylinder-afterbody juncture $\left(r/r_b = 0.505\right)$, a p_r/p_t value of 0.983 is obtained for a Mach number of 0.30 whereas a p_r/p_t value of only 0.857 is obtained for a Mach number of 1.00. Reference 5 shows that a low internal pressure results in the AID taking a less bluff shape and a consequent

degradation of the resulting drag coefficients. Thus, if the AID is to be an efficient subsonic decelerator, the inlets must be located at large enough values of r/r_b to insure adequate ram-air pressures which maintain the design shape.

Pressure drag coefficients obtained by integration of the pressure distributions of figure 4 are presented in figure 6 for the AID with burble fence and for the burble fence alone as a function of free-stream Mach number. The results indicate that the C_D values for the AID with the burble fence increase monotonically with an increase in Mach number from a value of 0.49 at a Mach number of 0.20 to a value of 0.915 at a Mach number of 1.00. The curve for the burble fence alone represents the integrated drag coefficients based on the projected frontal area of the burble fence. The burble fence is required for dynamic stability at certain subsonic Mach numbers, and the burble-fence drag coefficients are needed in the design program of reference 2. It is interesting to note that the burble-fence drag coefficient is highly dependent on Mach number at subsonic speeds. The C_D values increase with increase in Mach number in a manner similar to that noted for the afterbody with the fence attached. The C_D values increase from a value of -0.14 at a Mach number of 0.20 to a value of 0.615 at a Mach number of 1.00.

AID Shapes

Since AID configurations are constructed of a flexible fabric for normal application, the resulting AID shapes are dependent on the aerodynamic loading used in their design. Thus, sample AID shapes were derived for the pressure distributions and the burble-fence drag coefficients obtained in the experimental part of this investigation by using the design program of reference 2 to examine the effects of varying flow conditions on the resulting AID shapes. Shapes were derived using a recovery pressure ratio p_r/p_t of 1.0 and pressure distributions obtained at Mach numbers of 0.50, 0.85, and 1.00. These shapes are shown in figure 7 along with the original shape around which the pressure distributions were measured. The front surface of the resulting shapes are different, depending on the pressure distribution used in their derivation. Thus it is important that pressure distributions obtained at the correct flow conditions be used in designing AID shapes for subsonic deployment. The shape derived for the Mach 0.50 pressure distribution is relatively bluff and has a large surface slope over much of its front surface. The shapes become progressively less bluff with increase in Mach number. The experimental pressure-distribution model shape differed from any of the derived shapes and generally fell between the shapes derived for Mach 0.85 and 1.00 pressure data. However, the surface slope slightly forward of the $r/r_b = 1.00$ position is less than for either of the other shapes presented. Since the new shapes derived by use of the experimental pressure distributions are somewhat different from the shape about which the measurements were

made, the new shapes are only approximately correct. However, the $M_\infty = 0.85$ shape and the $M_\infty = 1.00$ shape are not vastly different from the experimental-model shape and are believed to be sufficiently accurate for deployment application in this Mach number region. More refined shapes could be obtained by measuring the pressure distributions about the approximate shapes and using them to calculate more accurate shapes. This procedure could be repeated to obtain shapes to any refinement required.

CONCLUSIONS

A wind-tunnel investigation was conducted at a free-stream Mach number from 0.20 to 1.00 on a solid model of an attached inflatable decelerator (AID) connected to the base of an ogive-cylinder. Tests were conducted to obtain ram-air and surface pressure distributions about the AID. The resulting pressure distributions were used in a design program to obtain new shapes which were compared with the original pressure-distribution shape. The results indicated the following:

1. The pressure-coefficient distributions indicate that a separated flow region exists near the intersection of the cylinder and the forward surface of the AID. Downstream of the point where the flow attaches to the AID, the surface pressure distributions are similar to those obtained for the AID without the ogive-cylinder forebody.

2. A ratio of ram-air pressure to free-stream total pressure as low as 0.857 is obtained near the middle of the front surface of the AID and increases to near 1.0 at the maximum radius of the AID. Thus, if the AID is to be an efficient decelerator with a high drag coefficient at subsonic speeds, the inlets must be located at the AID periphery to obtain the internal pressure required to maintain the design shape.

3. The drag coefficients for the AID increase monotonically with increasing Mach number from a value of 0.49 at a Mach number of 0.20 to a value of 0.915 at a Mach number of 1.00.

4. Since AID shapes derived for subsonic deployment are dependent on the pressure distributions used in their derivation, it is important that pressure distributions obtained at the correct flow conditions be used in the design of the AID shapes.

Langley Research Center,
National Aeronautics and Space Administration,
Hampton, Va., March 8, 1972.

REFERENCES

1. Guy, L. D.: Structural and Decelerator Design Options for Mars Entry. J. Spacecraft Rockets, vol. 6, no. 1, Jan. 1969, pp. 44-49.

2. Mikulas, Martin M., Jr.; and Bohon, Herman L.: Development Status of Attached Inflatable Decelerators. J. Spacecraft Rockets, vol. 6, no. 6, June 1969, pp. 654-660.

3. Deveikis, William D.; and Sawyer, James Wayne: Static Aerodynamic Characteristics, Pressure Distributions, and Ram-Air Inflation of Attached Inflatable Decelerator Models at Mach 3.0. NASA TN D-5816, 1970.

4. Bohon, Herman L.; and Miserentino, R.: Deployment and Performance Characteristics of 5-Foot-Diameter (1.5 m) Attached Inflatable Decelerators From Mach Number 2.2 to 4.4. NASA TN D-5840, 1970.

5. Bohon, Herman L.; and Miserentino, Robert: Attached Inflatable Decelerator Performance Evaluation and Mission-Application Study. AIAA Paper No. 70-1163, Sept. 1970.

6. Deveikis, William D.; and Sawyer, James Wayne: Flow Patterns and Pressure Distributions Around a Bluff Afterbody in the Wake of a 120° Cone for Various Separation Distances at Mach 3.0. NASA TN D-6281, 1971.

7. Barton, R. Reed: Development of Attached Inflatable Decelerators for Supersonic Application. GER-13680 (Contract No. NAS 1-7359), Goodyear Aerospace Corp., May 22, 1968. (Available as NASA CR-66613.)

8. Reichenau, David E. A.: Investigation of an Attached Inflatable Decelerator System for Drag Augmentation of the Voyager Entry Capsule at Supersonic Speeds. AEDC-TR-68-71, U.S. Air Force, Apr. 1968.

9. Baker, D. C.: Investigation of an Inflatable Decelerator Attached to a 120-deg Conical Entry Capsule at Mach Numbers From 2.55 to 4.40. AEDC-TR-68-227, U.S. Air Force, Oct. 1968.

10. Sawyer, James Wayne; and Whitcomb, Charles F.: Subsonic and Transonic Pressure Distributions Around a Bluff Afterbody in the Wake of a 120° Cone for Various Separation Distances. NASA TN D-6569, 1971.

11. Flatau, Abraham; Olson, Donald N; and Miller, Miles C.: The Use of an Attached Inflatable Decelerator for Store Delivery From High Speed Aircraft From Low Altitude. AIAA Paper No. 70-1199, Sept. 1970.

12. Ward, Vernon, G.; Whitcomb, Charles F.; and Pearson, Merwin D.: Air-Flow and Power Characteristics of the Langley 16-Foot Transonic Tunnel With Slotted Test Section. NACA RM L52E01, 1952.

TABLE I.- MODEL COORDINATES AND SURFACE PRESSURE COEFFICIENTS

Orifice	x/r_b	r/r_b	C_p				
			$M_\infty = 0.20$	$M_\infty = 0.30$	$M_\infty = 0.40$	$M_\infty = 0.50$	$M_\infty = 0.60$
1	-0.219	0.110	0.4985	0.5293	0.5454	0.5615	0.5785
2	-.119	.110	.5004	.5257	.5409	.5651	.5860
3	-.044	.110	.5698	.5808	.5914	.6188	.6583
4	-.000	.110	.5799	.5840	.6079	.6276	.6672
5	.007	.150	.5640	.5616	.5780	.5995	.6255
6	.026	.201	.5317	.5390	.5521	.5728	.6023
7	.046	.250	.5417	.5339	.5500	.5721	.6005
8	.066	.301	.5605	.5856	.5713	.6116	.6212
9	.087	.350	.6820	.6600	.6488	.7181	.6693
10	.109	.401	.7154	.6860	.7124	.7614	.7722
11	.124	.434	.7032	.6996	.7637	.8043	.7746
12	.136	.460	.7318	.7496	.7477	.8033	.7940
13	.156	.500	.7530	.7792	.7889	.7683	.8248
14	.187	.563	.6899	.7119	.7415	.7455	.7852
15	.220	.623	.5666	.5853	.5941	.6287	.6710
16	.251	.676	.4322	.4469	.4700	.5009	.5470
17	.285	.725	.3352	.3390	.3656	.3982	.4481
18	.320	.772	.1445	.1559	.1752	.2021	.2541
19	.357	.815	-.0426	-.0415	-.0086	.0145	.0592
20	.398	.857	-.1701	-.1467	-.1194	-.0905	-.0496
21	.443	.895	-.3481	-.3174	-.2935	-.2727	-.2392
22	.502	.934	-.4695	-.4382	-.4153	-.4000	-.3665
23	.580	.970	-.2971	-.2699	-.2391	-.1962	-.1236
24	.624	.984	-.0274	.0194	-.0522	.0980	.1650
25	.693	.997	.2069	.1942	.1910	.1935	.2198
26	.767	1.000					
27	.822	.991					
28	.874	.972	-.3645	-.3587	-.3601	-.3517	-.3228
29	.933	.934	-.3705	-.3743	-.3732	-.3670	-.3428
30	.973	.895	-.3736	-.3821	-.3766	-.3738	-.3504
31	.999	.856	-.3841	-.3899	-.3853	-.3692	-.3599
32	1.035	.772	-.3876	-.3881	-.3879	-.3743	-.3618
33	1.047	.675	-.3906	-.3838	-.3787	-.3688	-.3551
34	1.027	.565	-.3724	-.3843	-.3764	-.3689	-.3534
35	.955	.425	-.3925	-.3800	-.3758	-.3744	-.3493
36	.821	.300	-.3697	-.3506	-.3519	-.3420	-.3321
37	.694	.225	-.3288	-.3302	-.3331	-.3274	-.3114
38	.018	.175	.5205	.5387	.5549	.5763	.5993
39	.037	.225	.5174	.5307	.5432	.5653	.5828
40	.057	.275	.5205	.5330	.5508	.5657	.5866
41	.078	.326	.5329	.5695	.5762	.5825	.6099
42	.100	.376	.5926	.6103	.6252	.6163	.6499
43	.122	.426	.6204	.6361	.6570	.7032	.7089
44	.222	.627	.5410	.5649	.5721	.6102	.6547
45	.323	.775	.1255	.1514	.1654	.1923	.2373
46	.505	.937	-.4954	-.4697	-.4588	-.4512	-.4226
47	.727	1.012	.2844	.2248	.2195	.2302	.2503
48	.733	1.032	.2902	.3148	.3313	.3542	.3838
49	.741	1.050	-.1969	-.1072	-.0274	.0453	.1604
50	.758	1.073	-1.3996	-1.2920	-1.2028	-1.1319	-.9883
51	.778	1.087	-1.7768	-1.6495	-1.5321	-1.4996	-1.5272
52	.799	1.095	-1.6569	-1.3237	-.9834	-.7006	-.5754
53	.833	1.099	-.5028	-.4764	-.4844	-.4681	-.4308
54	.864	1.090	-.3734	-.3951	-.3974	-.3977	-.3706
55	.888	1.070	-.3716	-.3761	-.3795	-.3669	-.3560
56	.900	1.030	-.3628	-.3602	-.3679	-.3563	-.3470
57	.890	1.000	-.3690	-.3643	-.3593	-.3461	-.3390

TABLE I.- MODEL COORDINATES AND SURFACE PRESSURE COEFFICIENTS – Continued

Orifice	x/r_b	r/r_b	C_p				
			$M_\infty = 0.70$	$M_\infty = 0.80$	$M_\infty = 0.85$	$M_\infty = 0.90$	$M_\infty = 0.95$
1	-0.219	0.110	0.6098	0.6560	0.6768	0.6994	0.7371
2	-.119	.110	.6178	.6642	.6808	.7179	.7487
3	-.044	.110	.6753	.7246	.7370	.7666	.7975
4	-.000	.110	.6844	.7252	.7399	.7668	.8020
5	.007	.150	.6574	.6970	.7155	.7484	.7759
6	.026	.201	.6327	.6733	.6947	.7249	.7565
7	.046	.250	.6291	.6668	.6867	.7157	.7448
8	.066	.301	.6621	.6897	.7001	.7275	.7576
9	.087	.350	.7343	.7345	.7567	.7704	.8008
10	.109	.401	.8006	.7927	.8001	.8161	.8306
11	.124	.434	.8548	.8377	.8495	.8481	.8758
12	.136	.460	.8569	.8722	.8853	.8846	.9046
13	.156	.500	.8570	.9052	.9156	.9271	.9474
14	.187	.563	.8389	.8711	.9169	.9446	.9607
15	.220	.623	.7243	.7868	.8253	.8658	.9028
16	.251	.676	.6064	.6814	.7186	.7617	.8066
17	.285	.725	.5092	.5854	.6258	.6702	.7174
18	.320	.772	.3192	.4032	.4486	.4989	.5531
19	.357	.815	.1289	.2169	.2626	.3212	.3767
20	.398	.857	.0145	.0997	.1417	.1999	.2558
21	.443	.895	-.1781	-.1040	-.0612	-.0059	.0511
22	.502	.934	-.3056	-.2364	-.1991	-.1510	-.0996
23	.580	.970	-.0225	.0986	.1585	.2184	.2858
24	.624	.984	.2300	.3048	.3422	.3840	.4313
25	.693	.997	.2638	.3220	.3516	.3935	.4406
26	.767	1.000					
27	.822	.991					
28	.874	.972	-.3089	-.3039	-.3015	-.3035	-.2988
29	.933	.934	-.3265	-.3198	-.3177	-.3174	-.3135
30	.973	.895	-.3336	-.3261	-.3266	-.3227	-.3197
31	.989	.856	-.3370	-.3274	-.3305	-.3224	-.3214
32	1.035	.772	-.3399	-.3298	-.3315	-.3274	-.3229
33	1.047	.675	-.3364	-.3314	-.3250	-.3251	-.3208
34	1.027	.565	-.3360	-.3325	-.3231	-.3233	-.3196
35	.955	.425	-.3346	-.3304	-.3228	-.3160	-.3204
36	.821	.300	-.3190	-.3130	-.3030	-.3020	-.3055
37	.694	.225	-.3067	-.2984	-.2932	-.2901	-.2919
38	.018	.175	.6304	.6745	.6982	.7260	.7587
39	.037	.225	.6207	.6658	.6879	.7166	.7478
40	.057	.275	.6193	.6606	.6846	.7141	.7452
41	.078	.326	.6289	.6730	.6899	.7237	.7555
42	.100	.376	.6598	.6920	.7217	.7480	.7821
43	.122	.426	.7183	.7442	.7710	.7990	.8299
44	.222	.627	.6931	.7705	.7899	.8273	.8715
45	.323	.775	.3059	.3913	.4345	.4873	.5398
46	.525	.937	-.3536	-.2830	-.2408	-.1959	-.1423
47	.727	1.012	.2912	.3476	.3811	.4237	.4716
48	.733	1.032	.4312	.4827	.5159	.5525	.5952
49	.741	1.050	.2749	.3903	.4351	.4888	.5442
50	.758	1.073	-.7149	-.4403	-.3263	-.2178	-.1195
51	.778	1.087	-1.3259	-1.0034	-.8737	-.7467	-.6300
52	.799	1.095	-.5513	-.4871	-.4583	-.4450	-.4379
53	.823	1.099	-.2911	-.3743	-.3671	-.3600	-.3530
54	.864	1.090	-.3415	-.3349	-.3349	-.3303	-.3248
55	.888	1.070	-.3317	-.3253	-.3290	-.3222	-.3191
56	.900	1.030	-.3254	-.3195	-.3217	-.3194	-.3142
57	.890	1.000	-.3201	-.3185	-.3112	-.3136	-.3097

TABLE I.- MODEL COORDINATES AND SURFACE PRESSURE COEFFICIENTS – Concluded

Orifice	x/r_b	r/r_b	C_p				
			$M_\infty = 1.00$	$M_\infty = 0.80$	$M_\infty = 0.60$	$M_\infty = 0.40$	$M_\infty = 0.20$
1	-0.219	0.110	0.7747	0.6426	0.5786	0.5368	0.5178
2	-.119	.110	.7841	.6585	.5846	.5351	.5221
3	-.044	.110	.8324	.7169	.6482	.5890	.5519
4	-.000	.110	.8326	.7236	.6570	.5950	.5817
5	.007	.150	.8085	.6903	.6168	.5687	.5424
6	.026	.201	.7892	.6706	.5991	.5443	.5237
7	.046	.250	.7792	.6636	.5951	.5440	.5179
8	.066	.301	.7920	.6822	.6518	.5803	.5424
9	.087	.350	.8286	.7244	.6863	.6521	.6583
10	.109	.401	.8774	.7882	.7235	.6660	.6766
11	.124	.434	.9259	.8292	.7745	.7146	.6590
12	.136	.460	.9380	.8520	.8019	.7339	.6552
13	.156	.500	.9851	.8884	.8109	.7260	.7072
14	.187	.563	.9850	.8865	.7848	.6958	.6491
15	.220	.623	.9348	.7953	.6780	.5987	.5381
16	.251	.676	.8465	.6865	.5550	.4769	.4380
17	.285	.725	.7606	.5868	.4508	.3625	.3303
18	.320	.772	.6066	.4097	.2613	.1809	.1386
19	.357	.815	.4352	.2270	.0748	-.0047	-.0507
20	.398	.857	.3143	.1029	-.0467	-.1217	-.1853
21	.443	.895	.1120	-.1005	-.2398	-.3066	-.3508
22	.502	.934	-.0452	-.2269	-.3609	-.4208	-.4774
23	.560	.970	.3440	.0998	-.1260	-.2419	-.3141
24	.624	.984	.4827	.3081	.1628	.0492	-.0419
25	.693	.997	.4900	.3234	.2226	.1907	.1998
26	.767	1.000					
27	.822	.991					
28	.874	.972	-.3379	-.3080	-.3304	-.3533	-.3600
29	.933	.934	-.3555	-.3253	-.3443	-.3721	-.3718
30	.973	.895	-.3639	-.3329	-.3524	-.3774	-.3845
31	.999	.856	-.3666	-.3357	-.3561	-.3850	-.4120
32	1.035	.772	-.3664	-.3403	-.3606	-.3835	-.4038
33	1.047	.675	-.3633	-.3367	-.3603	-.3827	-.4055
34	1.027	.565	-.3629	-.3315	-.3615	-.3835	-.3702
35	.955	.425	-.3607	-.3340	-.3468	-.3770	-.3936
36	.821	.300	-.3450	-.3136	-.3272	-.3548	-.3629
37	.694	.225	-.3289	-.2975	-.3083	-.3317	-.3376
38	.018	.175	.7914	.6760	.5924	.5531	.5296
39	.037	.225	.7815	.6631	.5848	.5381	.5137
40	.057	.275	.7788	.6598	.5870	.5639	.5199
41	.078	.326	.7869	.6712	.6092	.5991	.5767
42	.100	.376	.8101	.7032	.6632	.6539	.6287
43	.122	.426	.8588	.7542	.7249	.7422	.6567
44	.222	.627	.9148	.7680	.6636	.6034	.5479
45	.323	.775	.5912	.4009	.2508	.1730	.1306
46	.505	.937	-.0795	-.2754	-.4118	-.4603	-.4934
47	.727	1.012	.5177	.3521	.2523	.2246	.2592
48	.733	1.032	.6379	.4903	.3896	.3401	.2841
49	.741	1.050	.5956	.3943	.1524	-.0356	-.2102
50	.758	1.073	-.0266	-.4287	-.9797	-1.1996	-1.3851
51	.778	1.087	-.5224	-.9891	-1.5234	-1.5428	-1.7799
52	.799	1.095	-.4850	-.4890	-.5995	-.9821	-1.6525
53	.823	1.099	-.3915	-.3806	-.4304	-.4826	-.5113
54	.864	1.090	-.3664	-.3437	-.3705	-.3999	-.3936
55	.888	1.070	-.3617	-.3344	-.3494	-.3826	-.3873
56	.900	1.030	-.3569	-.3299	-.3446	-.3659	-.3761
57	.890	1.000	-.3519	-.3219	-.3383	-.3629	-.3807

TABLE II.- RAM-AIR PRESSURE ORIFICE COORDINATES AND PRESSURE RATIOS[a]

M_∞	p_r/p_t for –			
	Orifice 58 $x/r_b = 0.129$ $r/r_b = 0.505$	Orifice 60 $x/r_b = 0.245$ $r/r_b = 0.714$	Orifice 61 $x/r_b = 0.322$ $r/r_b = 0.812$	Orifice 62 $x/r_b = 0.442$ $r/r_b = 0.926$
0.20	0.9925	0.9965	0.9978	0.9984
.30	.9825	.9945	.9945	.9968
.40	.9704	.9905	.9897	.9923
.50	.9575	.9874	.9852	.9898
.60	.9408	.9828	.9781	.9833
.70	.9174	.9779	.9702	.9753
.80	.8901	.9641	.9682	.9745
.85	.8820	.9609	.9618	.9713
.90	.8774	.9591	.9641	.9651
.95	.8659	.9556	.9573	.9674
1.00	.8572	.9510	.9564	.9663
.80	.8996	.9667	.9610	.9694
.60	.9414	.9811	.9768	.9823
.40	.9749	.9902	.9879	.9923
.20	.9911	.9965	.9969	.9975

[a]Orifice 59 was inoperative.

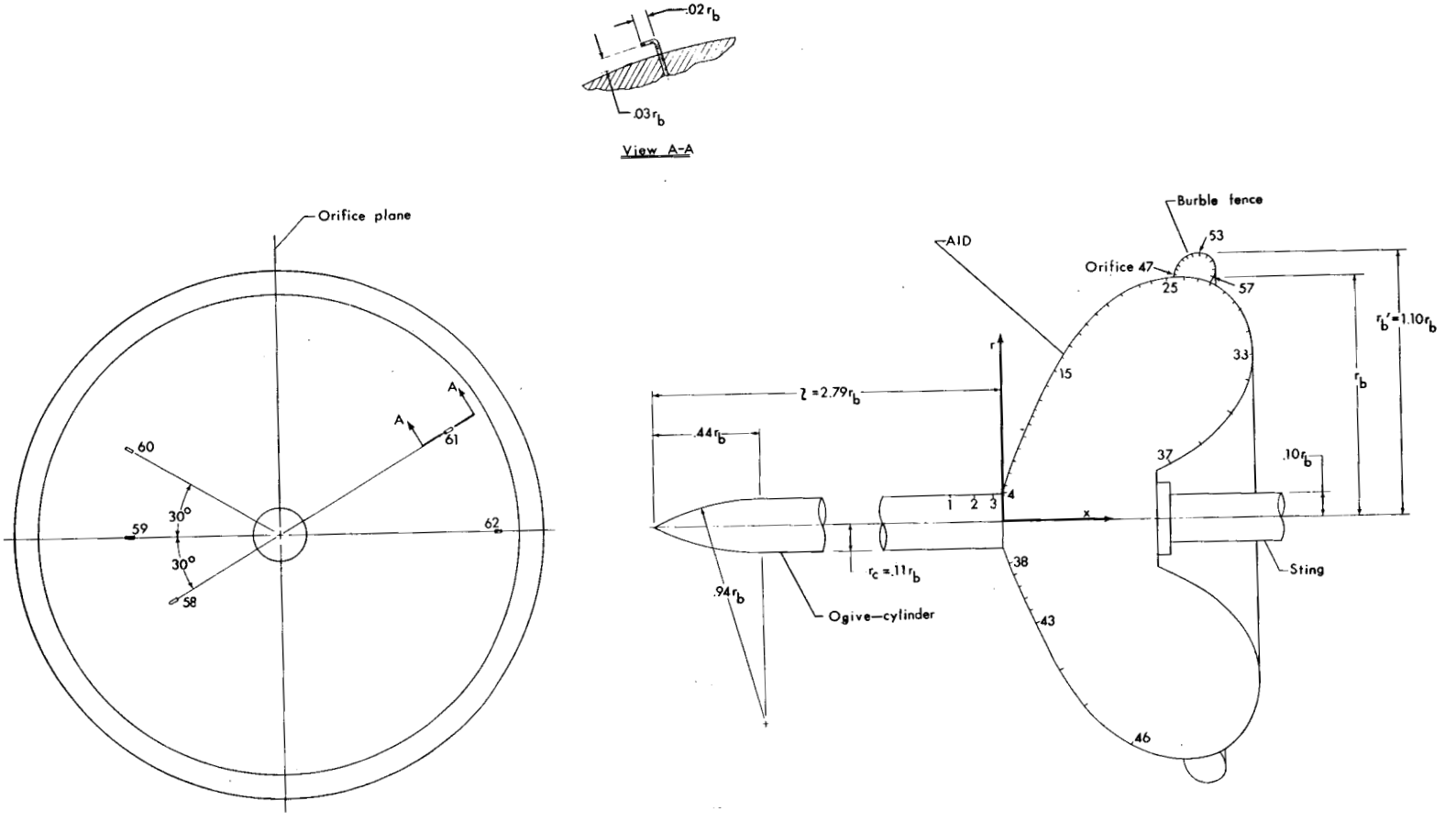

Figure 1.- Details of pressure-distribution model. r_b = 25.40 cm.

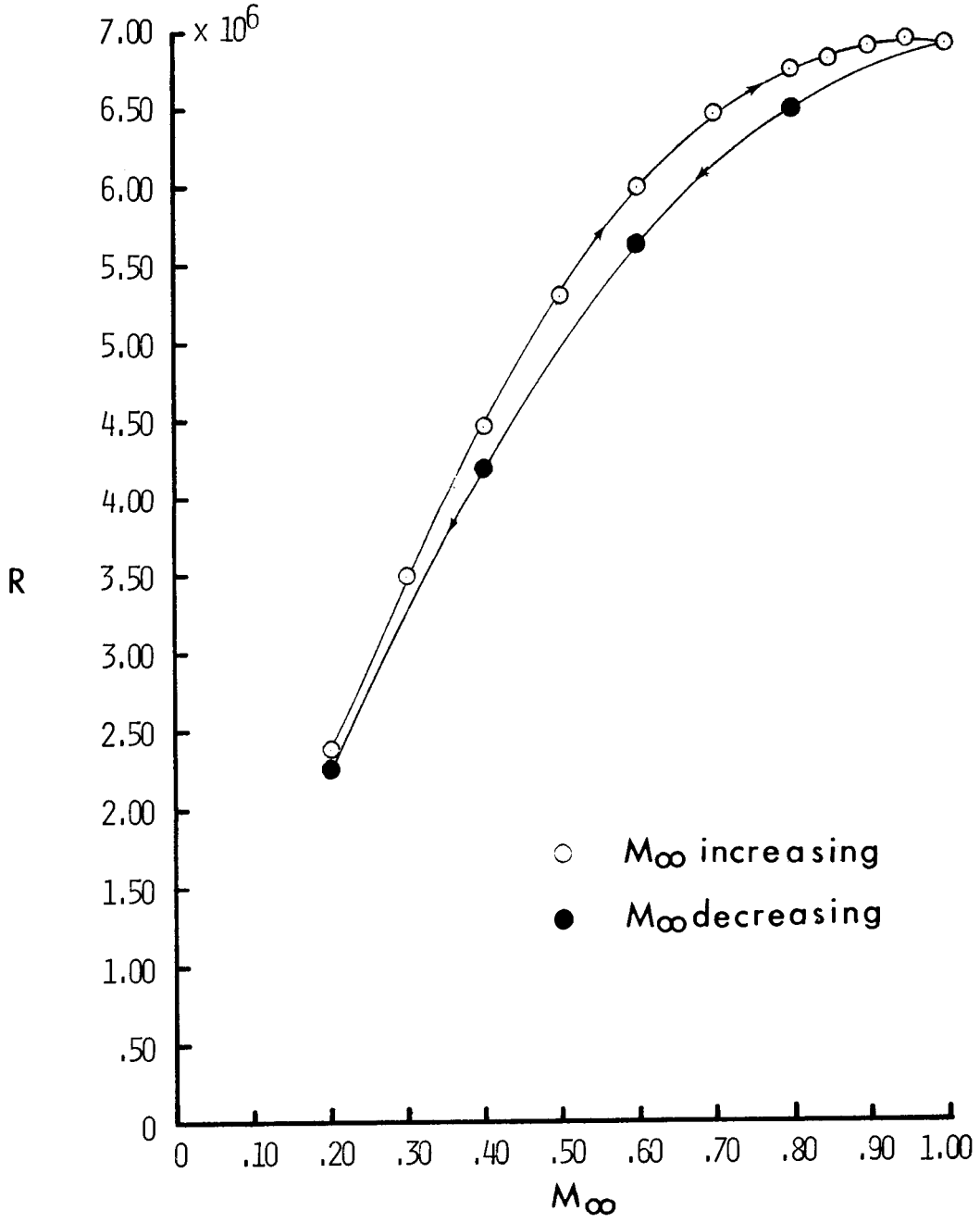

Figure 2.- Typical variation of Reynolds number with free-stream Mach number.

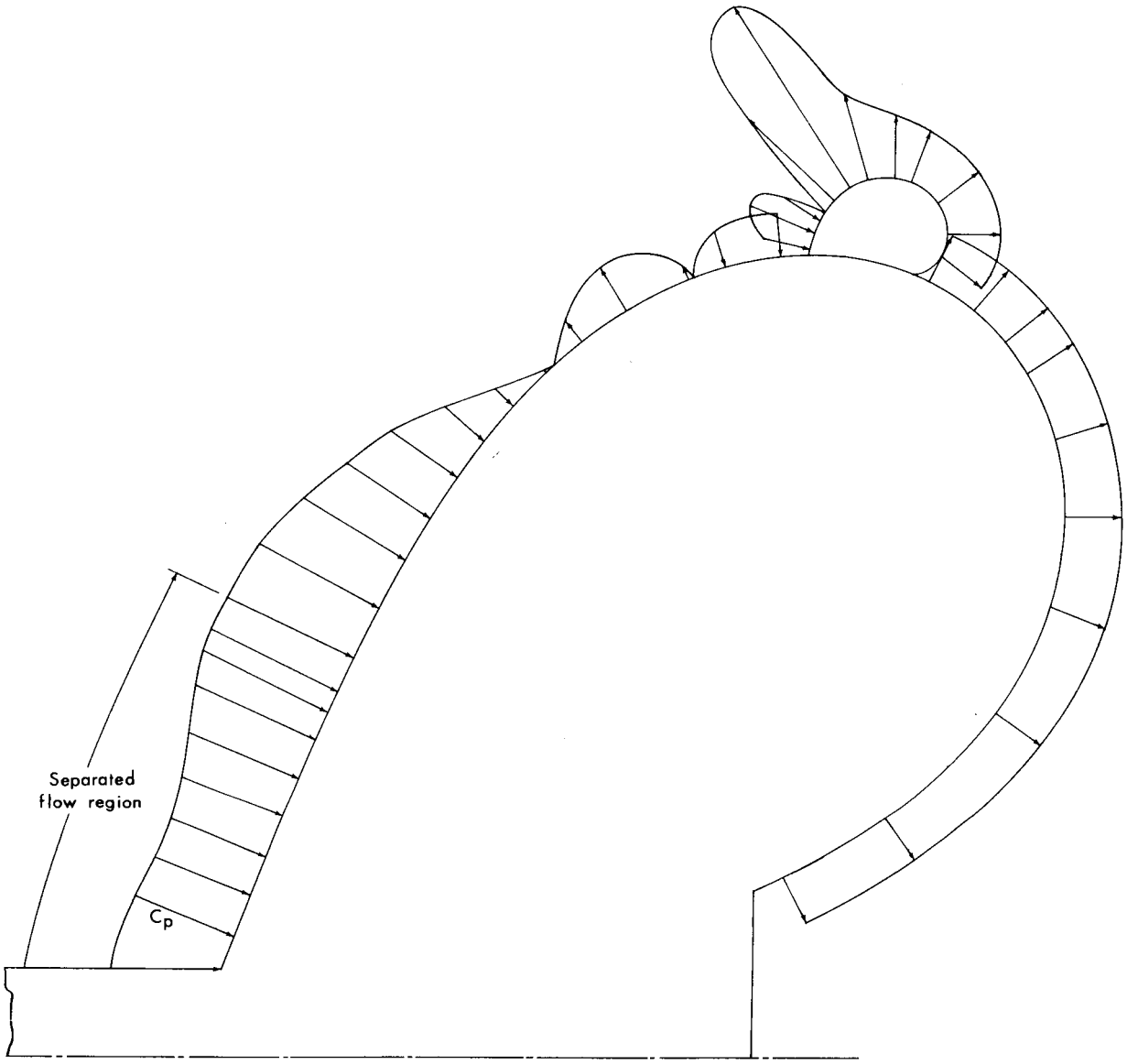

Figure 3.- Typical surface-pressure-coefficient distribution. $M_\infty = 0.70$.

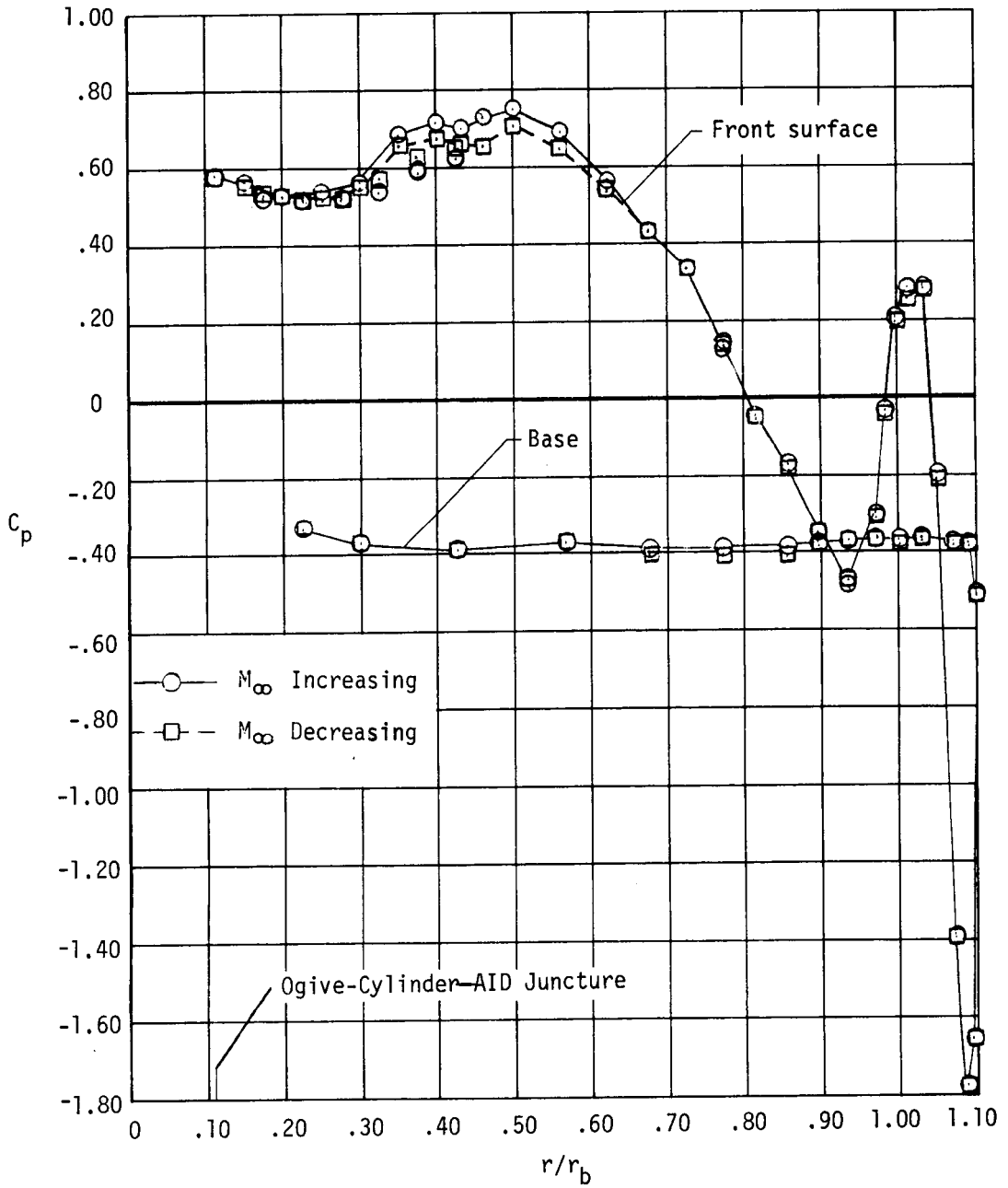

(a) $M_\infty = 0.20$.

Figure 4.- Experimental surface pressure distributions about AID attached to base of ogive-cylinder forebody.

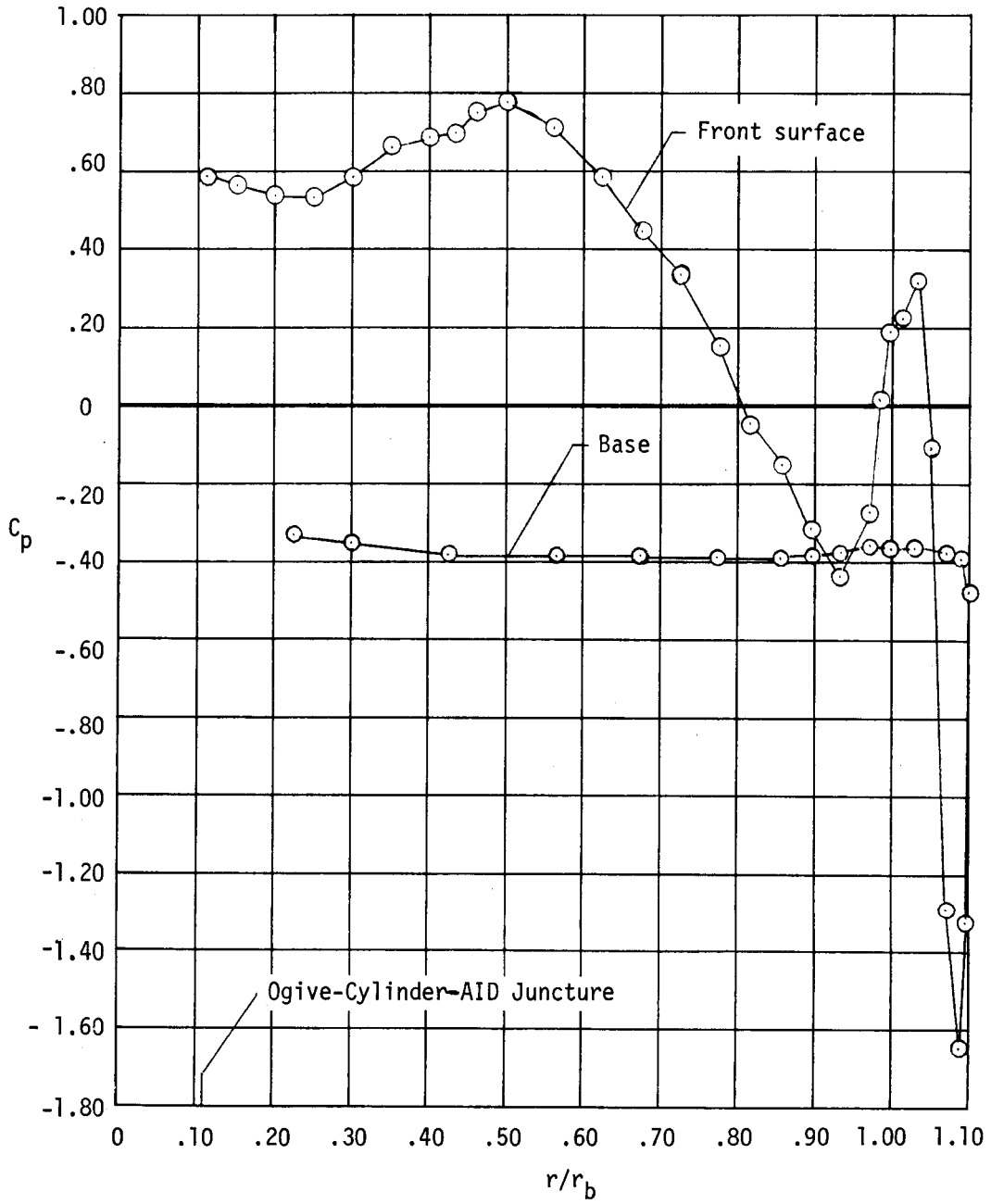

(b) $M_\infty = 0.30$.

Figure 4.- Continued.

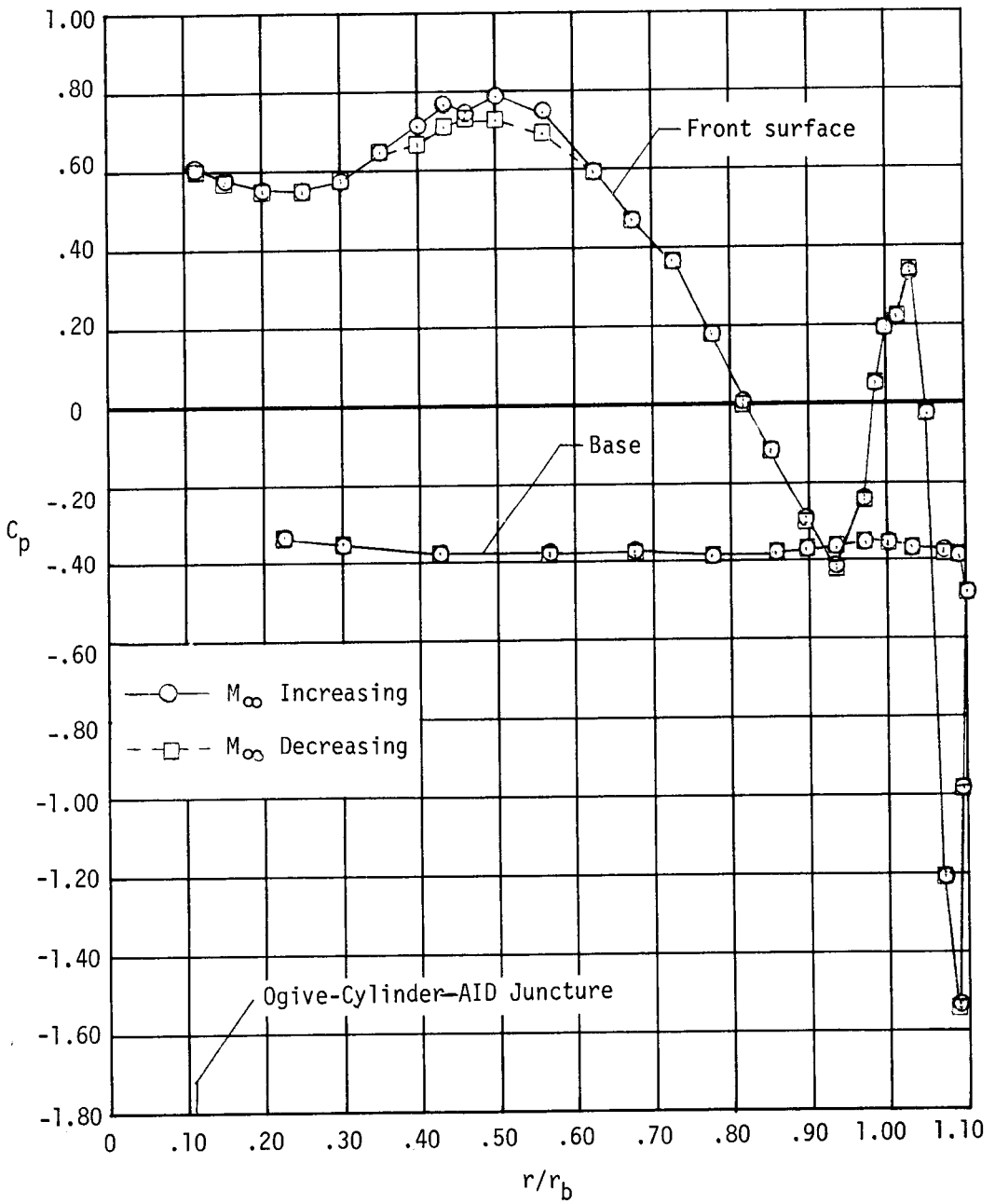

(c) $M_\infty = 0.40$.

Figure 4.- Continued.

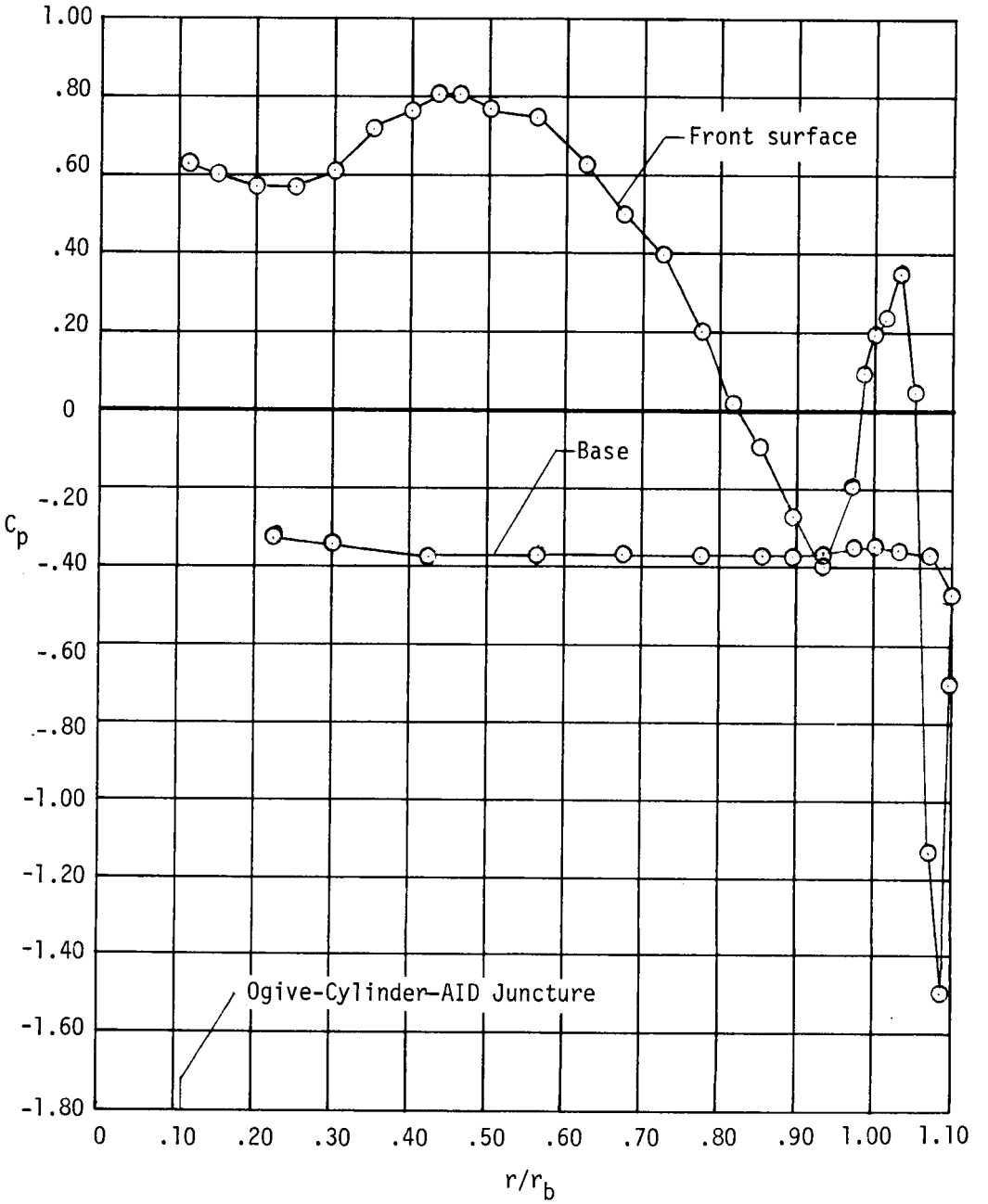

(d) $M_\infty = 0.50$.

Figure 4.- Continued.

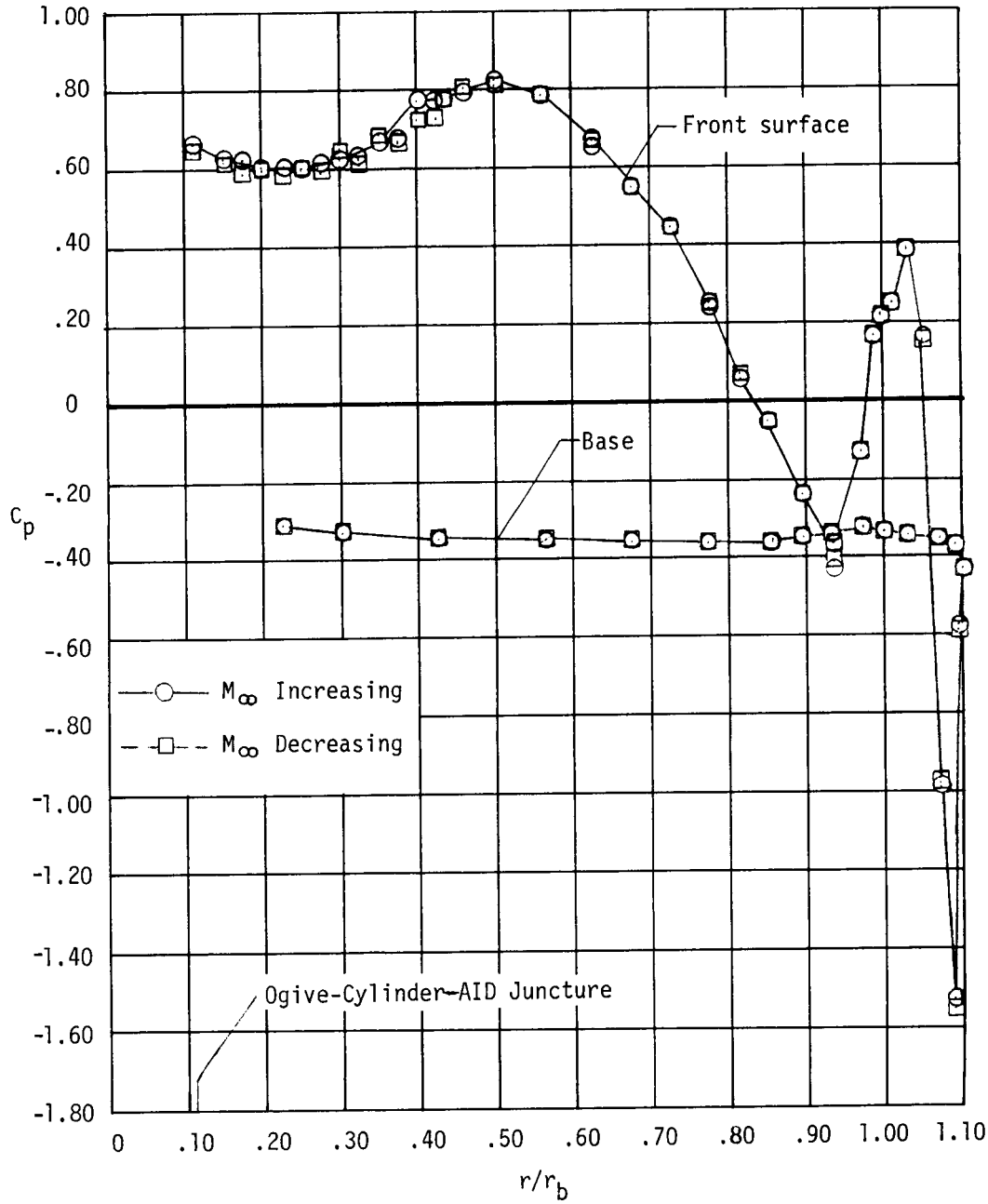

(e) $M_\infty = 0.60$.

Figure 4.- Continued.

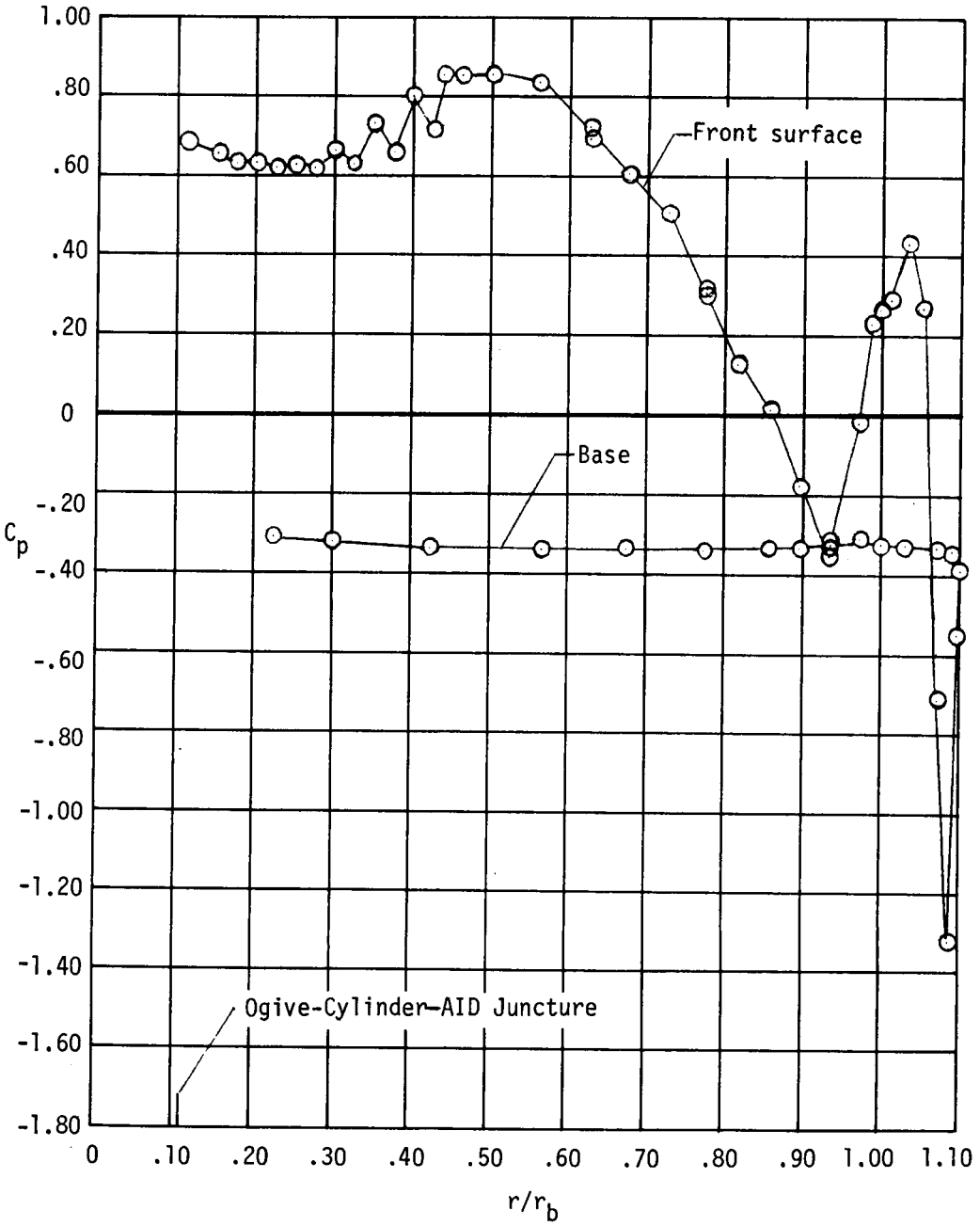

(f) $M_\infty = 0.70$.

Figure 4.- Continued.

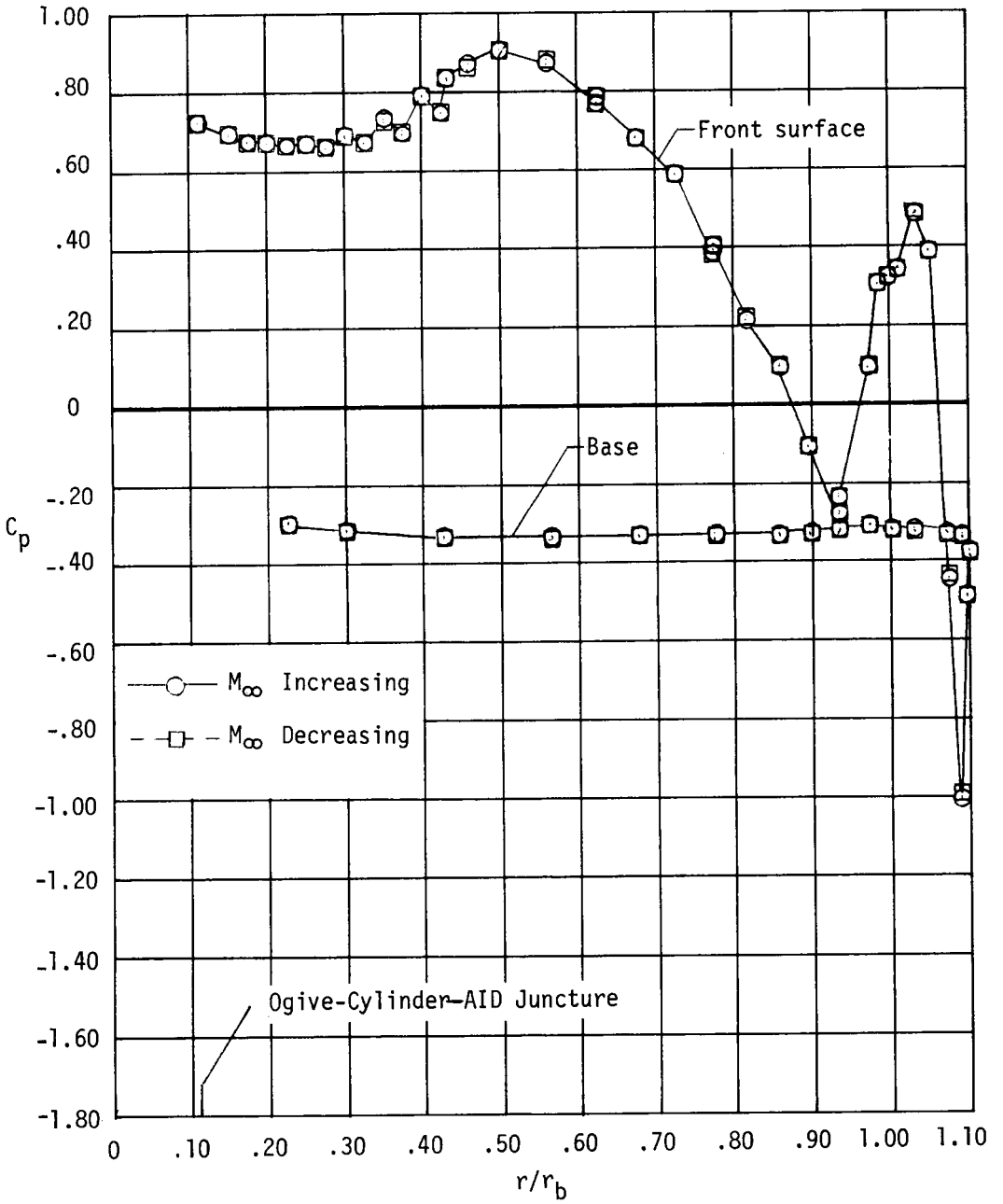

(g) $M_\infty = 0.80$.

Figure 4.- Continued.

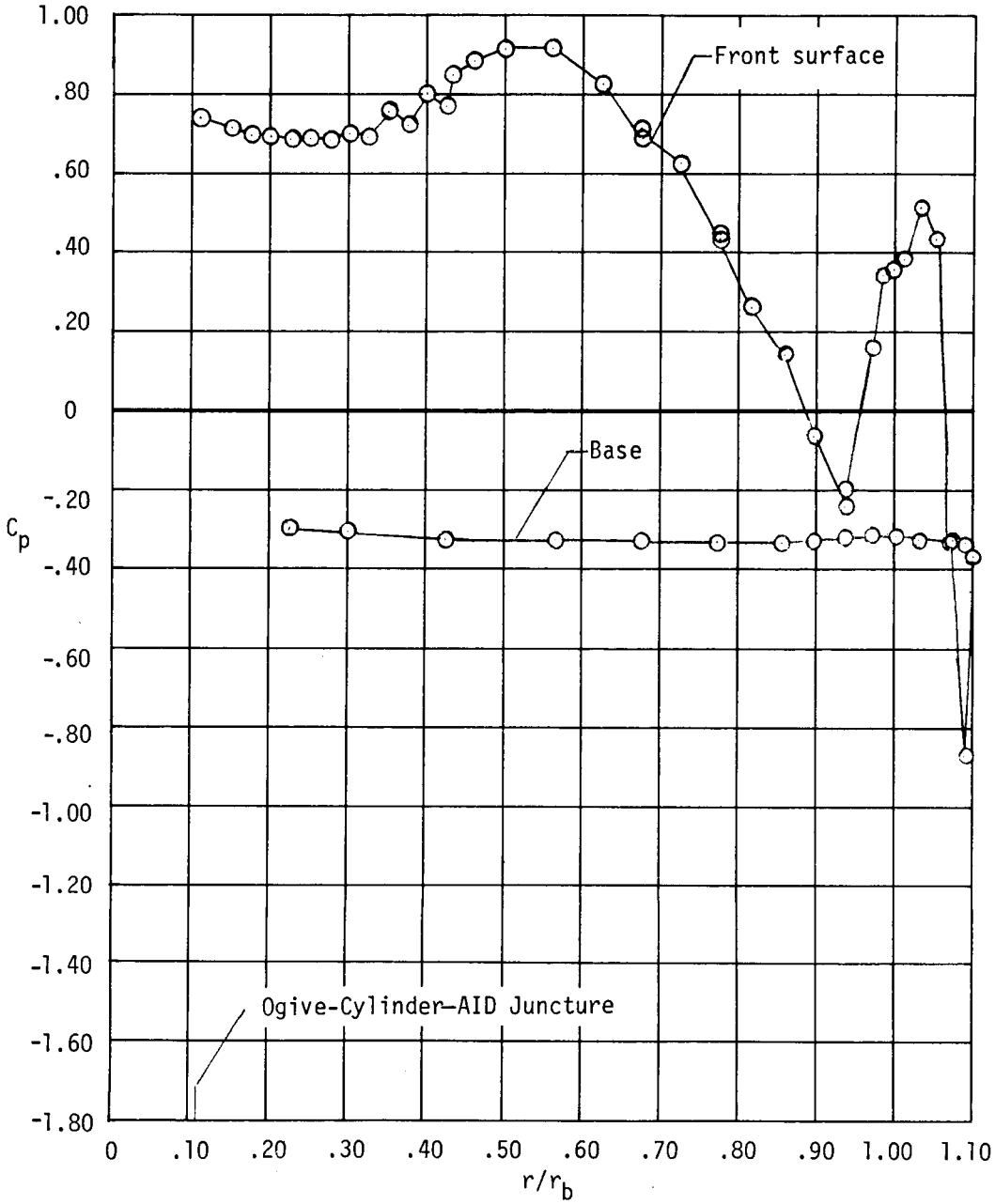

(h) $M_\infty = 0.85$.

Figure 4.- Continued.

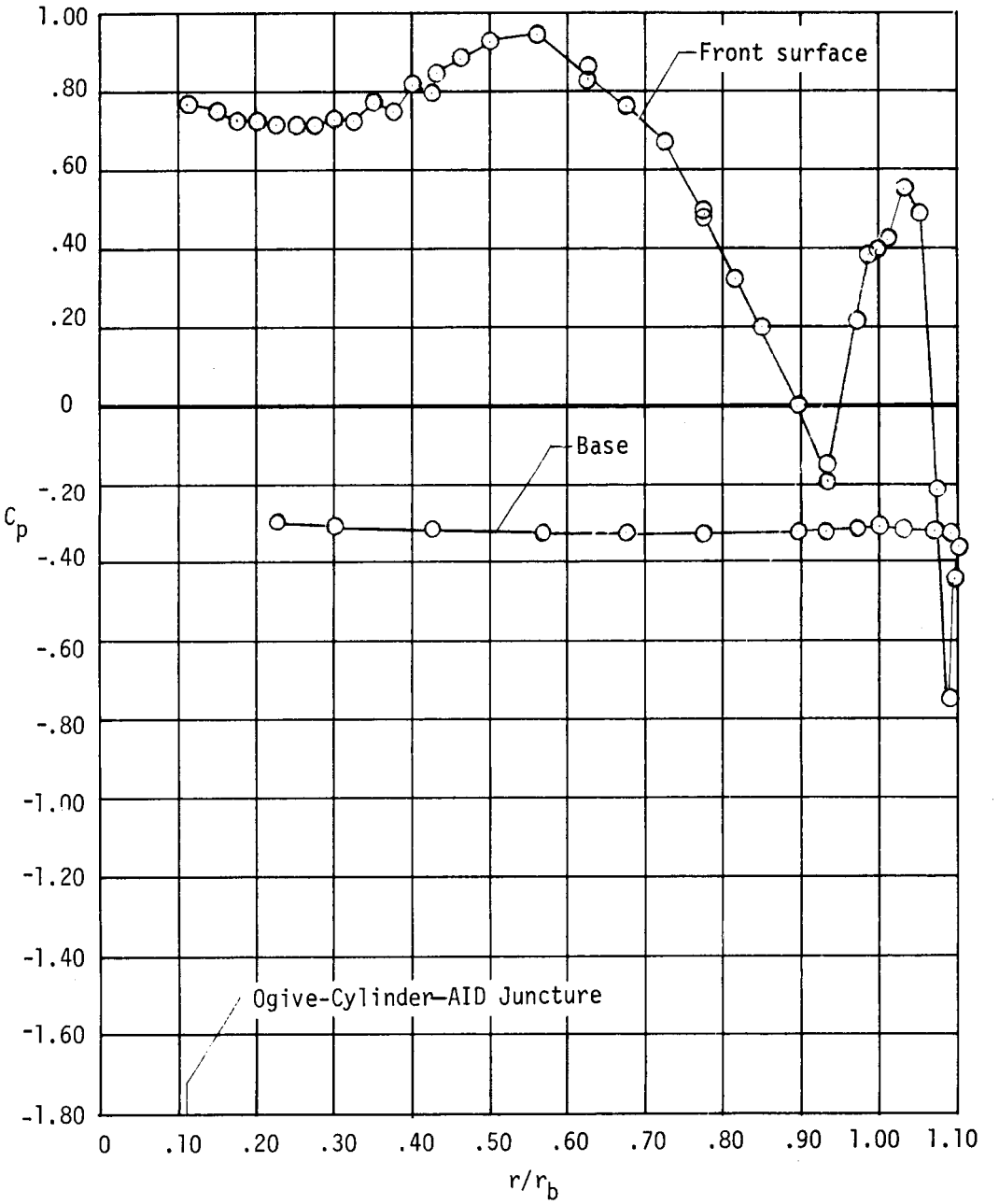

(i) $M_\infty = 0.90$.

Figure 4.- Continued.

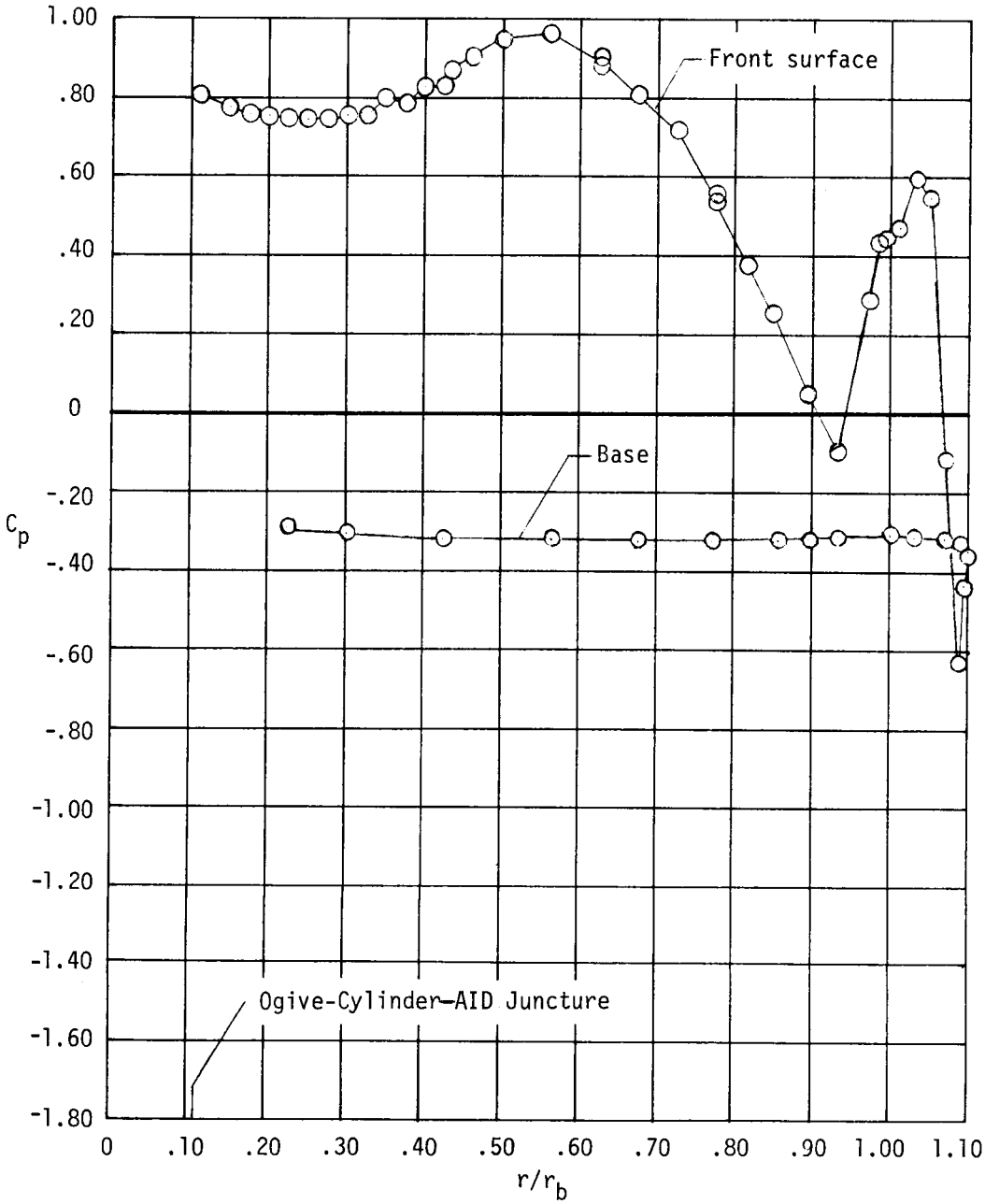

(j) $M_\infty = 0.95$.

Figure 4.- Continued.

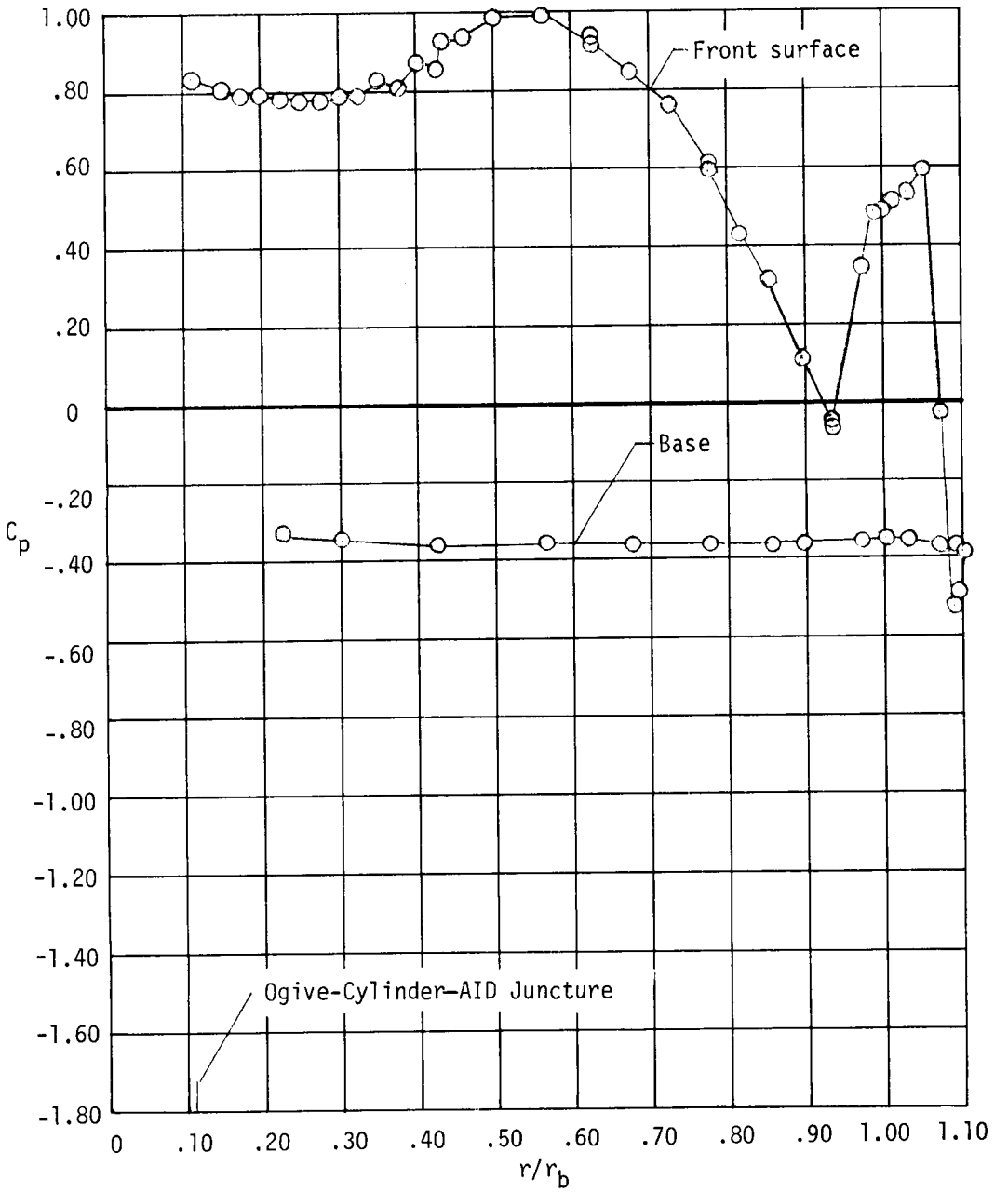

(k) $M_\infty = 1.00$.

Figure 4.- Concluded.

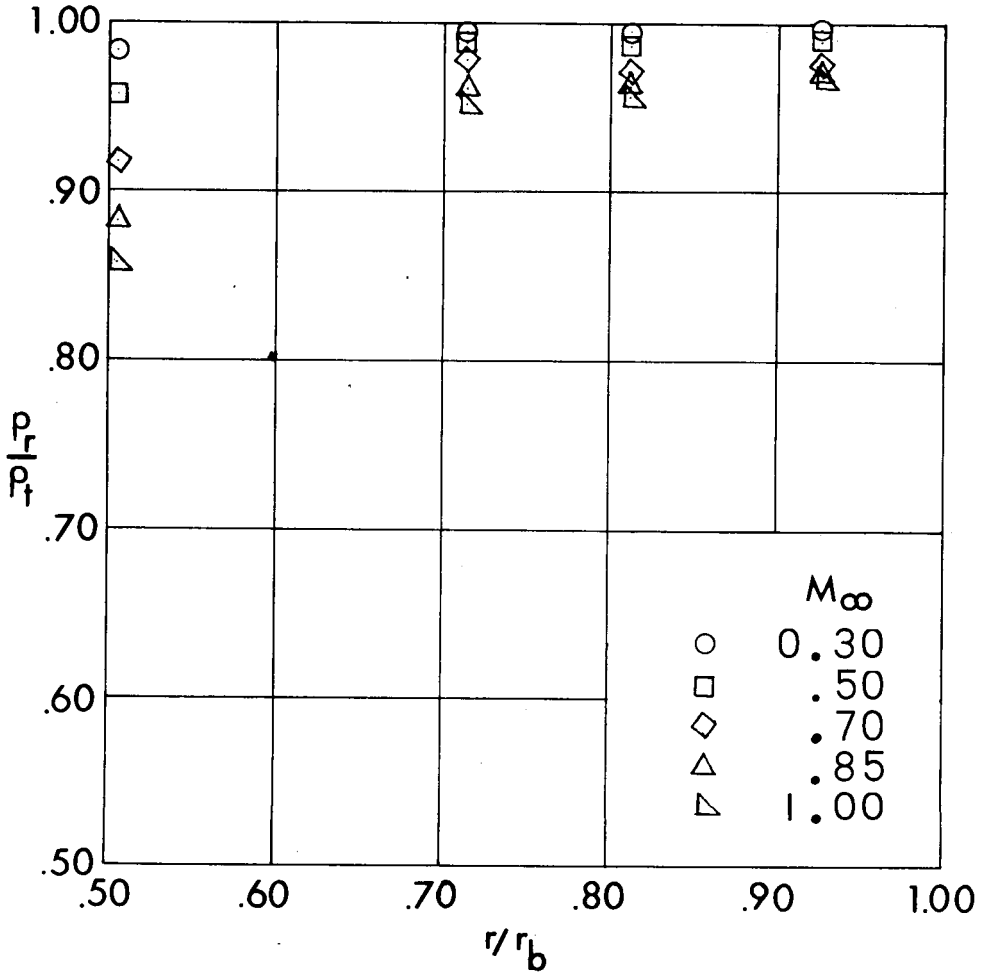

Figure 5.- Ram-air pressure distribution around AID attached to ogive-cylinder forebody.

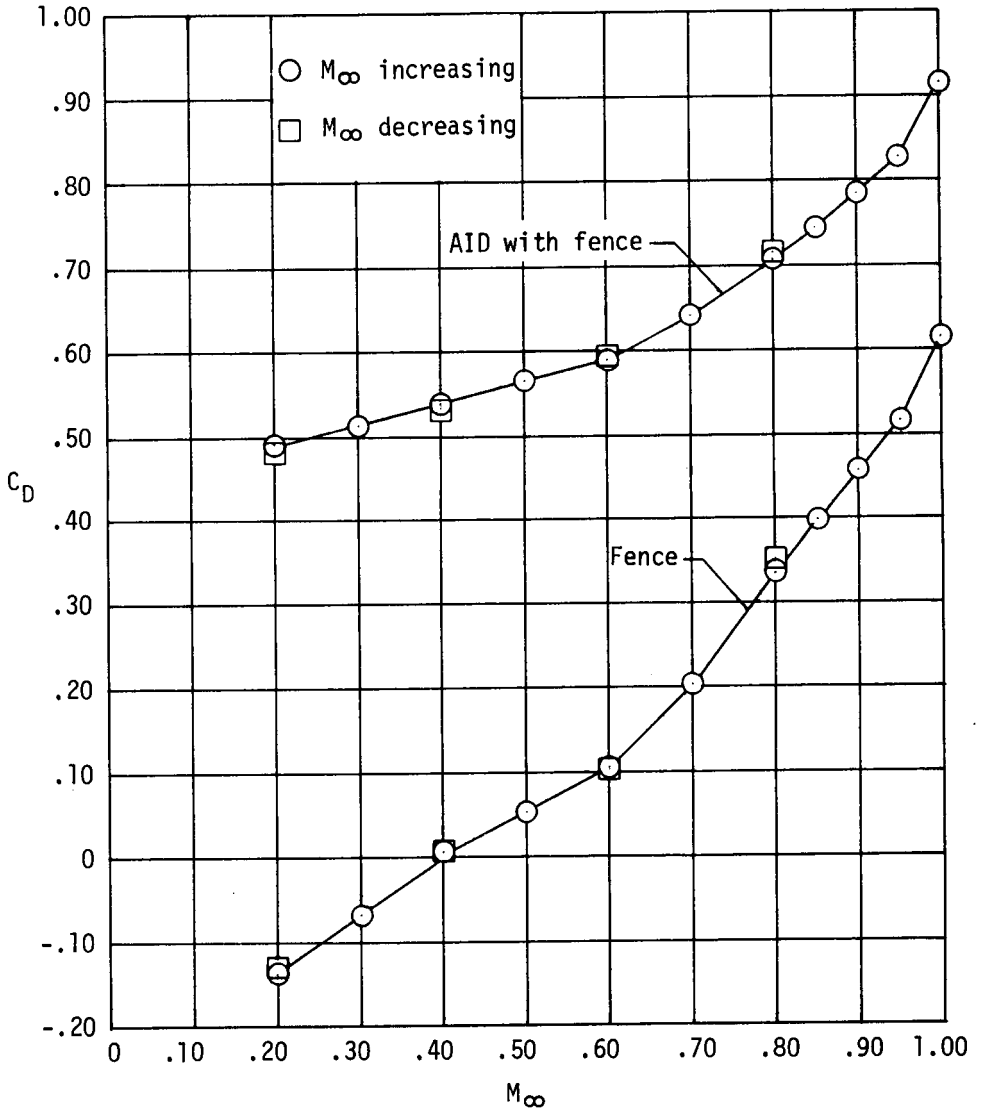

Figure 6.- AID and burble-fence pressure drag coefficients at various free-stream Mach numbers.

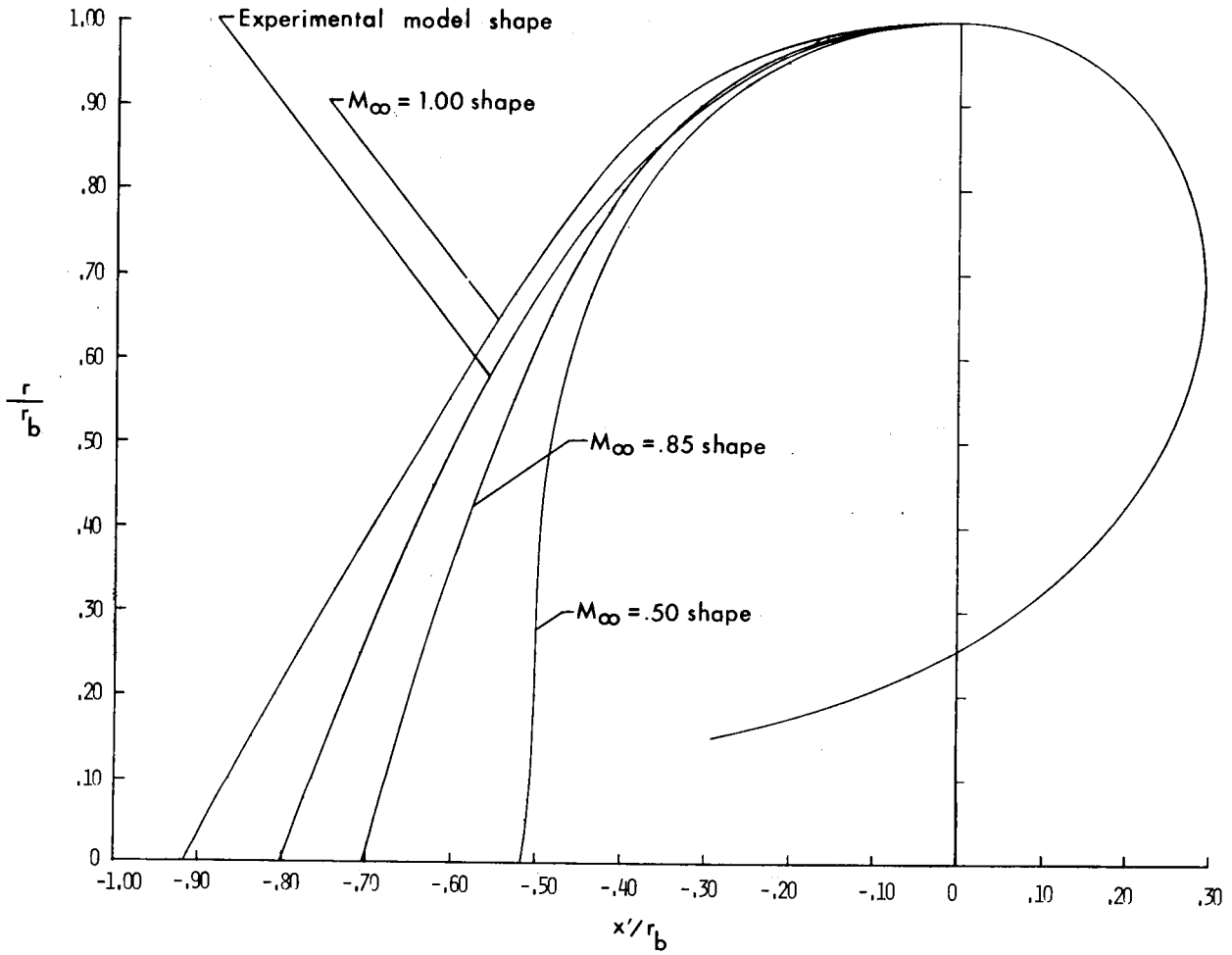

Figure 7.- Comparison of AID shapes as a function of free-stream Mach number.